Using Bayesian Optimization to Improve Solar Panel Performance by Developing Antireflective, Superomniphobic Glass

Sajad Haghanifar [1] **Bolong Cheng** [2] **Michael McCourt** [2] **Paul Leu** [1]

Abstract

Photovoltaic solar panel efficiency is dependent on photons transmitting through the glass sheet covering and into the crystalline silicon solar cells within. However, complications such as soiling and light reflection degrade performance. Our goal is to identify a fabrication process to produce glass which promotes photon transmission and is superomniphobic (repels fluids), for easier cleaning. In this paper, we propose adapting Bayesian optimization to efficiently search the space of possible glass fabrication strategies; in this search we balance three competing objectives (transmittance, haze and oil contact angle). We present the glass generated from this Bayesian optimization strategy and detail its properties relevant to photovoltaic solar power.

1. Introduction

Solar energy is a renewable form of energy which produces fewer emissions than fossil fuels and has potential to combat climate change (Hoffert et al., 2002; Creutzig et al., 2017). Photovoltaic (PV) solar panels, the most common solar energy deployment, come with various complications which have limited their widespread use. PV cells are protected by an encapsulant and a top glass sheet, which is used to protect the cells from moisture and the weather over its lifetime. However, this glass reflects about 4% of incident radiation. PV glass sheets are typically coated with a quarter wavelength thickness antireflection layer that reduces reflection losses at the air/glass interface (Shi et al., 2013). However, this coating does not provide for antireflection across a broad range of wavelengths or wide range of incidence angles. In addition, solar panels are subject to soiling which degrades their performance (He et al., 2011; Maghami et al., 2016; Mejia & Kleissl, 2013). Some strategies for dealing with this soiling issue include protecting the solar panels with dust shields (Mazumder et al., 2007), removing the particulate matter from the solar panels (Kawamoto & Shibata, 2015) and developing special types of glass/PET sheets with self-cleaning properties (Park et al., 2011).

In this work, we focus on fabricating high transmittance substrates which also have self-cleaning properties. We measure self-cleaning capacity through *superomniphobicity*, the ability to repel many liquids; superomniphobic surfaces demonstrate a static contact angle greater than 150° and low contact angle hysteresis for a variety of liquids (Pan et al., 2013; Choi et al., 2009; Tuteja et al., 2007; Kota et al., 2012). Other desirable properties include resistance to fogging (Mouterde et al., 2017; Wilke et al., 2018) and high durability against abrasion (Si et al., 2018).

Inspired by recent analysis of glasswing butterfly wings (Siddique et al., 2015), this research focuses on creating a new self-healing, durable, superomniphobic glass with *random* nanostructures as opposed to highly ordered subwavelength structure arrays. The glass is fabricated through a simple, scalable, two-step, maskless reactive ion etching and fluorination process, detailed in Section 2, which we demonstrate on 4 inch diameter glass wafers.

This fabrication process contains a large number of decisions (e.g., regarding the fluorination process) which impact the resulting glass in often complicated and unintuitive ways. We seek to guide these decisions to achieve ultrahigh transparency and ultralow haze without sacrificing superomniphobia. We turn to AI, specifically Bayesian optimization (Frazier, 2018), to adaptively search the space for effective fabrication strategies in a sample-efficient fashion. In Section 3, we phrase our search process as a multiobjective problem, introduce Bayesian optimization, and explain the necessary adaptations to serve our purpose. In Section 4, we detail the glass properties associated with one of the discovered fabrication strategies with the desired properties.

2. Fabrication Strategy

The nanofabrication process is performed in two steps: (a) reactive ion etching (RIE) and (b) plasma enhanced

[1]Laboratory for Advanced Materials at Pittsburgh, University of Pittsburgh, Pittsburgh, PA, USA [2]SigOpt, San Francisco, CA, USA. Correspondence to: Michael McCourt <mccourt@sigopt.com>.

Proceedings of the 36^{th} International Conference on Machine Learning, Long Beach, California, PMLR 97, 2019.

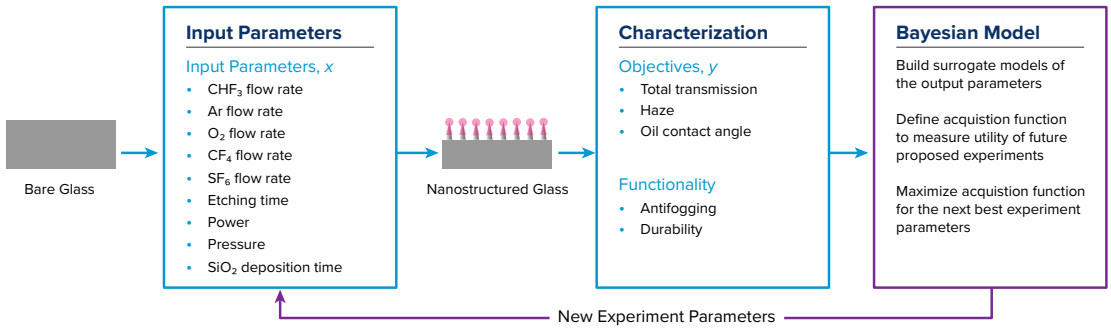

Figure 1. Schematic of experimental fabrication and Bayesian learning optimization process for nanostructured glass.

chemical vapor deposition (PECVD) and surface treatment with fluorination. This fabrication process scalably creates the nanostructures directly into the fused silica glass without the need for patterning or an external mask (Haghanifar et al., 2017; 2018). The first fabrication step focuses on RIE to create sub-wavelength nanostructures in the fused silica in order to maximize the total transparency and minimize the haze at the wavelength of 550 nm. The second processing step focuses on creating re-entrant structures and a low energy surface: in this processing step, we consider the deposition of silicon dioxide (SiO_2) by PECVD on top of the sub-wavelength nanostructures in order to make the structure re-entrant followed by fluorination. The complete fabrication details are too numerous for this extended abstract, but they can be obtained by contacting the authors. As limited by the fabrication hardware, we can consider only up to 5 simultaneous fabrications.

3. Bayesian Optimization for Efficient Search

Within the fabrication strategy detailed in Section 2, there are numerous decisions which must be made, e.g., the duration of the RIE. Figure 1 depicts the input parameters and objectives under analysis, and suggests the feedback loop with which we search over input parameters. We treat this as a multiobjective optimization problem with solution $\mathbf{x}^*$,

$$x^* \text{ satisfies } \begin{cases} x^* = \arg\max_{x\in\mathcal{X}} \ \theta_o(x), \\ x^* = \arg\max_{x\in\mathcal{X}} \ T_{\text{total}}(x), \text{ and} \\ x^* = \arg\min_{x\in\mathcal{X}} \ H(x), \end{cases} \quad (1)$$

where $\mathcal{X}$ is the space of all possible choices of the fabrication process parameters, $T_{\text{total}} : \mathcal{X} \to \mathbb{R}$ is the total transmission of 550 nm light through the resulting glass, $H : \mathcal{X} \to \mathbb{R}$ is the haze of that glass for 550 nm light and $\theta_o : \mathcal{X} \to \mathbb{R}$ is the ethylene glycol (oil) contact angle.

In general, there is no unique structure x^* that is simultaneously optimal in all the objectives in (1). In lieu of such a point, the solution to such a multiobjective problem is often defined as the Pareto-optimal set, or Pareto-efficient frontier $\mathcal{P} \in \mathcal{X}$. A more thorough explanation of the topic can be found in multicriteria literature (Ehrgott, 2005).

Bayesian optimization (BO) is a sample-efficient iterative search framework, where the relationship between process parameters and objective function values is unknown, and function evaluations (executing the fabrication and characterizing the resulting substrate) are expensive or time consuming. Standard BO has two components: a probabilistic *surrogate model*, to model the objective function f, and an *acquisition function*, to determine which x parameters to next sample. We build independent Gaussian processes (Fasshauer & McCourt, 2015) models of θ_o, T_{total} and H with mean functions identically zero and square-exponential covariance kernels length-scales in each dimension. The second component of BO involves optimizing the acquisition function—a utility function that measures the benefit of sampling at different points within $\mathcal{X}$, given what data has already been observed.

The basic BO strategy must be adapted to fit this multiobjective scenario, as well as to conform to the physical limitations of the fabrication process. All of the details are too numerous to describe here, but we highlight one key concept: not all of the points on $\mathcal{P}$ are relevant. Our new glass must perform better in all metrics than standard glass; consequently, we imposed performance thresholds $\theta_o(x) \geq 60°$, $T_{\text{total}}(x) \geq 88.5$ and $H(x) \leq 1.1$. To respect these thresholds we adapt the ϵ-*constraint method* (Hwang & Masud, 1979) to produce the scalar optimization problem:

$$\max_{x\in\mathcal{X}} T_{\text{total}}(x), \text{ s.t. } H(x) \leq \hat{H}, \theta_o(x) \geq \hat{\theta}_o,$$

with the analogous constrained scalar optimization problems also defined for θ_o and H. Our goal became to find as many points as possible on $\mathcal{P}$ which satisfy these constraints.

4. Results

After 64 fabrications driven by Bayesian optimization (which, itself, was seeded with 79 fabrications executed prior to the start of this project) we produced 5 points on

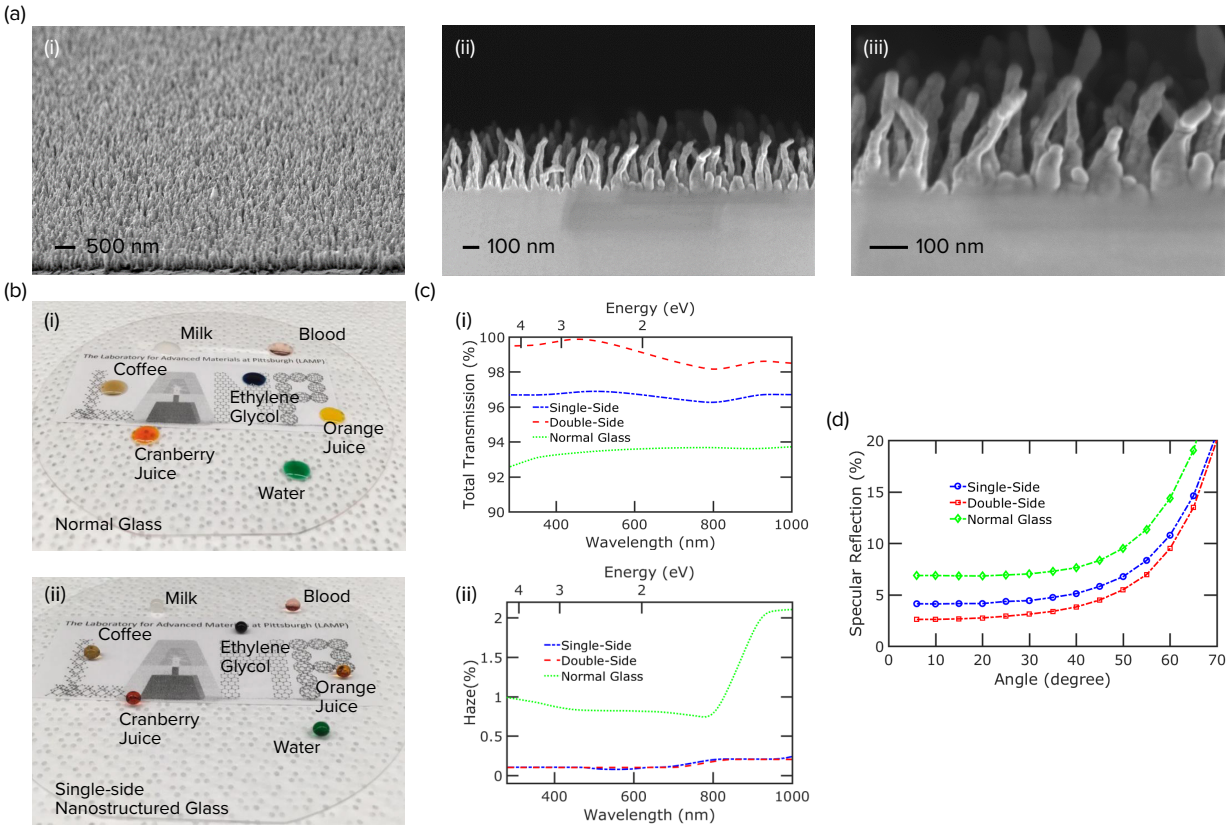

Figure 2. (a) shows (i) 20° tilted, (ii) and (iii) cross sectional SEM images of fabricated glass with different magnifications. (b) shows the droplet of different liquids on (i) normal and (ii) our superomniphobic glass. (c) (i) show transmission and (ii) haze plots as a function of wavelength for bare, single side and double side etched glass. The wavelength domain shown here is representative of the key range for most photovoltaic cells. (d) Angle-resolved spectra for reflection at 550 nm wavelength for bare, single side and double side etched glass.

Transmission (%)	Haze (%)	Oil Contact Angle (°)
97.01	**0.01**	**155**
95.90	0.03	157
95.65	0.02	156
94.54	1.30	158
94.36	0.60	158

Table 1. The Pareto efficient points found during the fabrication search. The point in bold is the point for which the characterization detailed in Figure 2 was conducted.

$\mathcal{P}$; all of these points were not present in the original 79 fabrications. They are presented in Table 1.

Figure 2(a) shows scanning electron microscopy (SEM) images of the sub-wavelength, re-entrant structures. The randomness in the height and spacing provide for broadband and omnidirectional antireflection, like the glasswing butterfly wings (Siddique et al., 2015). By depositing the SiO_2, the surface area at the top of the pillars increase which provide the re-entrant structures required for omniphobicity.

To investigate the omniphobic property, we deposited 5 μl drops of different liquids with different surface tensions, from water (72.8 mN/m) to ethylene glycol (47.7 mN/m), on both bare (Figure 2(b)(i)) and nanostructured (Figure 2(b)(ii)) substrates. The bare fused silica has $42.9 \pm 1.1°$ and $18.7 \pm 0.7°$ contact angle for water and oil. By creating re-entrant structure on the bare fused silica, the water and contact angles increase significantly to $162.1 \pm 2.0°$ and $155.2 \pm 2.2°$, respectively.

Figure 2(c) shows the transmission and haze results for glass as a function of wavelength. The total transmission of double-side nanostructured glass at 550 nm is 99.5%. This wavelength is the key wavelength for solar panels, and we can see a clear improvement in antireflection for this new glass which will translate to significant improvement for solar energy efficiency (Chen et al., 2012). In both single-side and double-side nanostructured glass, the haze value reduces to less than 0.1% across a broadband range of wavelength. Figure 2(d) shows the angle dependent specular reflection at 550 nm wavelength. The reflection values are always less than glass even for a high incidence angle of 70°, which reveals the high omnidirectional, antireflective performance of our fabricated glass.

References

Chen, C.-C., Dou, L., Zhu, R., Chung, C.-H., Song, T.-B., Zheng, Y. B., Hawks, S., Li, G., Weiss, P. S., and Yang, Y. Visibly Transparent Polymer Solar Cells Produced by Solution Processing. *ACS Nano*, 6(8):7185–7190, August 2012.

Choi, W., Tuteja, A., Chhatre, S., Mabry, J. M., Cohen, R. E., and McKinley, G. H. Fabrics with Tunable Oleophobicity. *Advanced Materials*, 21(21):2190–2195, June 2009.

Creutzig, F., Agoston, P., Goldschmidt, J. C., Luderer, G., Nemet, G., and Pietzcker, R. C. The underestimated potential of solar energy to mitigate climate change. *Nature Energy*, 2:17140, 8 2017.

Ehrgott, M. *Multicriteria optimization*, volume 491. Springer Science & Business Media, 2005.

Fasshauer, G. E. and McCourt, M. J. *Kernel-based Approximation Methods Using Matlab*. World Scientific, 2015.

Frazier, P. I. Bayesian optimization. In *Recent Advances in Optimization and Modeling of Contemporary Problems*, pp. 255–278. INFORMS, 2018.

Haghanifar, S., Gao, T., Vecchis, R. T. R. D., Pafchek, B., Jacobs, T. D. B., and Leu, P. W. Ultrahigh-transparency, ultrahigh-haze nanograss glass with fluid-induced switchable haze. *Optica*, 4(12):1522–1525, December 2017.

Haghanifar, S., Vecchis, R. T. R. D., Kim, K.-J., Wuenschell, J., Sharma, S. P., Ping Lu, Ohodnicki, P., and Leu, P. W. Flexible nanograss with highest combination of transparency and haze for optoelectronic plastic substrates. *Nanotechnology*, 29(42):42LT01, 2018.

He, G., Zhou, C., and Li, Z. Review of self-cleaning method for solar cell array. *Procedia Engineering*, 16:640–645, 2011.

Hoffert, M. I., Caldeira, K., Benford, G., Criswell, D. R., Green, C., Herzog, H., Jain, A. K., Kheshgi, H. S., Lackner, K. S., Lewis, J. S., Lightfoot, H. D., Manheimer, W., Mankins, J. C., Mauel, M. E., Perkins, L. J., Schlesinger, M. E., Volk, T., and Wigley, T. M. L. Advanced technology paths to global climate stability: Energy for a greenhouse planet. *Science*, 298(5595):981–987, 2002.

Hwang, C. and Masud, A. *Multiple objective decision making, methods and applications: a state-of-the-art survey*. Lecture notes in economics and mathematical systems. Springer-Verlag, 1979.

Kawamoto, H. and Shibata, T. Electrostatic cleaning system for removal of sand from solar panels. *Journal of Electrostatics*, 73:65–70, 2015.

Kota, A. K., Li, Y., Mabry, J. M., and Tuteja, A. Hierarchically Structured Superoleophobic Surfaces with Ultralow Contact Angle Hysteresis. *Advanced Materials*, 24(43): 5838–5843, 2012.

Maghami, M. R., Hizam, H., Gomes, C., Radzi, M. A., Rezadad, M. I., and Hajighorbani, S. Power loss due to soiling on solar panel: A review. *Renewable and Sustainable Energy Reviews*, 59:1307–1316, 2016.

Mazumder, M., Sharma, R., Biris, A., Zhang, J., Calle, C., and Zahn, M. Self-cleaning transparent dust shields for protecting solar panels and other devices. *Particulate Science and Technology*, 25(1):5–20, 2007.

Mejia, F. A. and Kleissl, J. Soiling losses for solar photovoltaic systems in california. *Solar Energy*, 95:357–363, 2013.

Mouterde, T., Lehoucq, G., Xavier, S., Checco, A., Black, C. T., Rahman, A., Midavaine, T., Clanet, C., and Qur, D. Antifogging abilities of model nanotextures. *Nature Materials*, 16(6):658–663, June 2017.

Pan, S., Kota, A. K., Mabry, J. M., and Tuteja, A. Superomniphobic Surfaces for Effective Chemical Shielding. *Journal of the American Chemical Society*, 135(2):578–581, January 2013. ISSN 0002-7863.

Park, Y.-B., Im, H., Im, M., and Choi, Y.-K. Self-cleaning effect of highly water-repellent microshell structures for solar cell applications. *Journal of Materials Chemistry*, 21(3):633–636, 2011.

Shi, E., Li, H., Yang, L., Zhang, L., Li, Z., Li, P., Shang, Y., Wu, S., Li, X., Wei, J., Wang, K., Zhu, H., Wu, D., Fang, Y., and Cao, A. Colloidal Antireflection Coating Improves GrapheneSilicon Solar Cells. *Nano Letters*, 13 (4):1776–1781, April 2013.

Si, Y., Dong, Z., and Jiang, L. Bioinspired Designs of Superhydrophobic and Superhydrophilic Materials. *ACS Central Science*, 4(9):1102–1112, September 2018.

Siddique, R. H., Gomard, G., and Hölscher, H. The role of random nanostructures for the omnidirectional antireflection properties of the glasswing butterfly. *Nature Communications*, 6:6909, April 2015.

Tuteja, A., Choi, W., Ma, M., Mabry, J. M., Mazzella, S. A., Rutledge, G. C., McKinley, G. H., and Cohen, R. E. Designing Superoleophobic Surfaces. *Science*, 318(5856): 1618–1622, December 2007.

Wilke, K. L., Preston, D. J., Lu, Z., and Wang, E. N. Toward Condensation-Resistant Omniphobic Surfaces. *ACS Nano*, 12(11):11013–11021, November 2018.